



Synthesis and characterization of Co–La–Zr–B quaternary amorphous nano alloy: Kinetic study for hydrogen generation from hydrolysis of sodium borohydride



Mohammad Hassan Loghmani, Abdollah Fallah Shojaei *

Department of Chemistry, Faculty of Science, University of Guilan, P.O. Box 1914, Rasht, Iran

ARTICLE INFO

Article history:

Received 24 February 2013
Received in revised form 3 May 2013
Accepted 13 May 2013
Available online 21 May 2013

Keywords:

Quaternary amorphous nano alloy
Co–La–Zr–B
Hydrogen generation
NaBH₄
Kinetic

ABSTRACT

Co–La–Zr–B quaternary amorphous nano alloy was for the first time prepared in situ ultrasound-assisted reduction of Co(II), La(III) and Zr(IV) chloride by sodium borohydride aqueous solution. Obtained powder was characterized by XRD, BET, ICP, FE-SEM and TEM techniques. No distinct peak could be observed in XRD pattern of the obtained alloy indicating that the Co–La–Zr–B possessed amorphous structure. Regarding to the size, SEM and TEM images depict that the most of particles are lower than 10 nm and there is no significant aggregation. Co–La–Zr–B nano alloy is highly active catalysts for hydrogen generation from the hydrolysis of sodium borohydride. The reported work also includes the full experimental details for the collection of a wealth of kinetic data to determine the activation energy ($E_a = 60.06$ - kJ mol^{-1}) and effects of the catalyst dosage, amount of substrate, and temperature on the rate for the catalytic hydrolysis of sodium borohydride. Catalytic hydrolysis of NaBH₄ is first order with respect to the catalyst concentration and zero order respect to the NaBH₄ concentration in the case of Co–La–Zr–B quaternary amorphous nano alloy.

© 2013 Elsevier B.V. All rights reserved.

1. Introduction

Nanoscale particle research has recently become a very important field in materials science. Such metal nanoparticles often exhibit very interesting electronic, magnetic, optical, and chemical properties. Amorphous alloy catalysts have received much attention owing to their higher activity, better selectivity, and stronger sulfur resistance in many hydrogenation reactions. Their unique features depend on their size, shape, surface composition, and surface atomic arrangement [1]. Sodium borohydride, NaBH₄, is the focus of interest since the late 1990s because of its stability in alkaline solutions, non-flammability, non-toxicity, environmental safety and the high theoretical hydrogen content [2–4]. NaBH₄ yields hydrogen gas and water-soluble sodium metaborate, NaBO₂, upon hydrolysis in the presence of certain catalysts. (Eq. (1)):



It is also the least expensive metal hydride readily available commercially, and it is currently one of the best candidates for use in portable devices [5]. It is found that metal borides were good catalysts for the hydrolysis reaction, of which cobalt boride Co–B was paid considerable attention for its good catalytic activity, low cost

and simple preparation method. The efficiency of hydrogen production can be significantly enhanced by using solid state catalysts such as precious metals Pt [6], Pd [7] and Ru [8], or transition metals and their salts like Mg-based alloy [9], Raney Ni and Co, nickel and cobalt borides [10–12]. Chemical reduction is most frequently used in preparing Co–B amorphous alloys [13–17]; however, the regular Co–B samples obtained via direct reduction of cobalt salt solution with a sodium borohydride solution usually display low surface area, broadly distributed particle size, and poor thermal stability against crystallization due to aggregation, because the reduction reaction is vigorous and exothermic [18,19]. Ultrasonication has proven a useful technique for inducing chemical reaction and inhibiting particle agglomeration due to the chemical effects from acoustic cavitation, which produces unusual chemical environments [20–23]. Previous papers proved that the alloy catalysts in the form of Co–Ni–B [24], Co–P–B [25], Co–Ni–P–B [26], and Co–Cr–B [27] exhibit superior catalytic activity as compared to Co–B catalyst in hydrogen production by hydrolysis of NaBH₄. Previously, Yuan and co-workers [28] have synthesized amorphous Co–Zr–B, having a nearly spherical morphology with diameters <50 nm. To the best of our knowledge, Co–La–Zr–B nano alloy has not been synthesized up to now. In this work, Co–La–Zr–B quaternary nano alloy was for the first time prepared in situ ultrasound-assisted reduction of Co(II), La(III) and Zr(IV) chloride by sodium borohydride aqueous solution. Indeed, zerovalent metal nanoscale of Cobalt, Zirconium and Lanthanum are prepared under Argon atmosphere and reflux

* Corresponding author. Tel.: +98 131 3233262.

E-mail address: shoja47@gmail.com (A.F. Shojaei).

condition. The obtained materials were characterized by XRD, BET, ICP, FE-SEM, EDS and TEM techniques. Activity of Co–B and Co–La–Zr–B powders were tested for hydrogen generation through hydrolysis of sodium borohydride alkaline solution. In order to approach the rate law for hydrogen generation several parameters were studied.

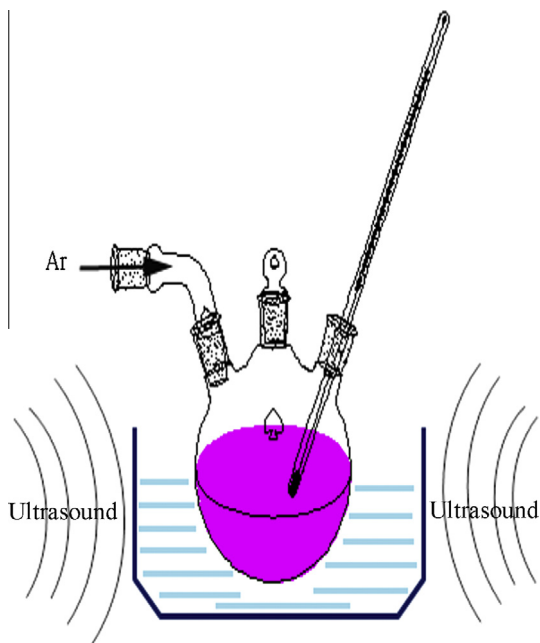
2. Experimental

2.1. Synthesis of Co–La–Zr–B amorphous nano alloy

Co–La–Zr–B amorphous nano alloy was prepared under Ar atmosphere, as shown in Scheme 1. In the typical synthesis, in 250 ml three-necked round bottom flask, 238 mg (1 mmol) of $\text{CoCl}_2 \cdot 6\text{H}_2\text{O}$, 371 mg (1 mmol) of $\text{LaCl}_3 \cdot 7\text{H}_2\text{O}$ and 233 mg (1 mmol) of ZrCl_4 were dissolved in 30 ml deionized water. Color of solution is purple at this moment. Then, the mixture was purged by pure Ar to remove oxygen molecules. Under sonicating condition 5 ml of sodium borohydride solution (5 mmol = 190 mg NaBH_4 in deionized water) was added drop by drop into metals solution. By addition of NaBH_4 solution, abrupt color change from purple to black indicates that the formation of metal nanoparticles was completed. The fine black precipitate, which was subsequently formed in the mixed solution, was filtrated out through vacuum-assisted filtration and washed repeatedly in distilled water. Then it was washed further with acetone, and dried at room temperature. Co–B is also synthesized by same method without Lanthanum and Zirconium salts.

2.2. Hydrogen generation by amorphous nano alloy

The kinetic studies with prepared catalysts were carried out in batch operation. A 50 ml two-necked round-bottom flask was used as the reactor. The left-neck port was equipped with a thermometer inserted into the solution to monitor the temperature, and the middle-neck port was fitted with an outlet to collect the evolved hydrogen gas. The hydrogen generated was collected by an inverted and water-filled cylinder. Hydrogen volume was measured by monitoring the water displacement from the cylinder as the reaction proceeded. No stirring was undertaken during the reaction as hydrogen evolution induced enough mixing effect. In order to establish the rate law for the catalytic hydrolysis of NaBH_4 using Co–La–Zr–B amorphous nano alloy, three different sets of experiments were performed. In the first set of experiments, the concentration of NaBH_4 was kept constant at 5 wt%, and the Co–La–Zr–B alloy dosage was varied in the range of 12.5, 25, and 50 mg. In the second set of experiments, Co–La–Zr–B dosage was held constant at 50 mg while the NaBH_4 concentration was varied in the range of 2.5, 5 and 10 wt.%. The third set of experiments was performed by keeping NaBH_4 and Co–La–Zr–B concentrations constant at 5 wt.% and 50 mg, respectively, and testing the temperature effect at 20, 30, 40 and 50 °C. Although the self-hydrolysis of sodium borohydride at room temperature is quite slow, it can be completely suppressed by working in highly basic solution [29]. Based on this, all experiments were performed in 2 wt.% NaOH concentration.



Scheme 1. Preparation procedure of Co–La–Zr–B amorphous nano alloy.

2.3. Characterization methods

XRD patterns were recorded by a D8 Bruker Advanced, X-ray diffractometer using $\text{Cu K}\alpha$ radiation ($\lambda = 1.54 \text{ \AA}$). The patterns were collected in the range $20\text{--}70^\circ 2\theta$ and continuous scan mode. Transmission electron microscope (TEM) image was obtained on a Philips CM10 transmission electron microscope with an accelerating voltage of 100 kV. Scanning image was obtained on a FE-SEM (field emission scanning electron microscope) Hitachi S-4160 microscope. The Cobalt, Lanthanum and Zirconium content of the samples were determined by ICP-OES (Inductively Coupled Plasma Optical Emission Spectroscopy, Leeman-Direct Reading Echelle). Specific surface areas of catalysts were measured by the BET method analysis under N_2 adsorptive (SIBATA SA 1100) after degassing.

3. Results and discussions

3.1. Characterization of the amorphous nano alloy

XRD patterns of Co–B and Co–La–Zr–B amorphous nano alloy are shown in Fig. 1. No distinct peak could be observed in XRD patterns indicating that the Co–B and Co–La–Zr–B alloy possessed amorphous phase. On the other hand, there is not any peak of Co_3O_4 , La_2O_3 , ZrO_2 and B_2O_3 in XRD pattern indicating formation of metal oxide is inhibited under Ar atmosphere. For more investigation, temperature controlling was conducted and results are shown in Fig. 2. All patterns recorded after 3 h calcination in electrical furnace. Fig. 2a and b shows XRD pattern of Co–B and Co–La–Zr–B samples were heated at 200 °C and air atmosphere.

As seen, there is not observed any peak even at 200 °C. Fig. 2c–e shows XRD patterns of Co–La–Zr–B nano powder at 300, 400 and 500 °C, respectively. It can be found that, an even temperature increase up to 500 °C Co–La–Zr–B is amorphous and no distinct peak could be observed. Fig. 2f shows XRD pattern of Co–B alloy at 500 °C. As shown, observed peaks are corresponded to Co_3O_4 phase. Indeed, Co–B can be oxidized to Co_3O_4 at 500 °C [30]. It can be concluded that, from comparison of Fig. 2e and f, Lanthanum and Zirconium ions prevent crystallization of Co_3O_4 phase. Co–La–Zr–B is also heated at 500 °C under Ar atmosphere and corresponded XRD pattern is shown in Fig. 2g. However, Co–La–Zr–B quaternary nano alloy has amorphous phase at this temperature. Specific surface areas and elemental analysis of catalysts are shown in Table 1. The surface area of Co–La–Zr–B is larger than Co–B. This indicates that addition of La and Zr can prevent particle agglomeration and thus increase the BET surface area of catalysts. The Cobalt, Lanthanum and Zirconium content of the catalyst were determined by ICP-OES and EDS. For ICP analysis, Co–La–Zr–B powder was dissolved in boiled aqua regia solution, HNO_3/HCl (1/3 ratio). Since the ICP-OES analysis indicates the presence of Cobalt, Lanthanum and Zirconium in the sample with Co/La, Co/Zr and La/Zr molar ratios 0.9, 1.1 and 0.7, respectively. More

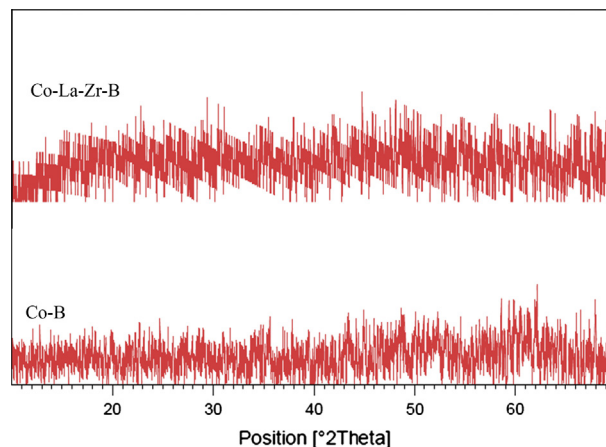


Fig. 1. XRD pattern of Co–B and Co–La–Zr–B amorphous nano alloys.

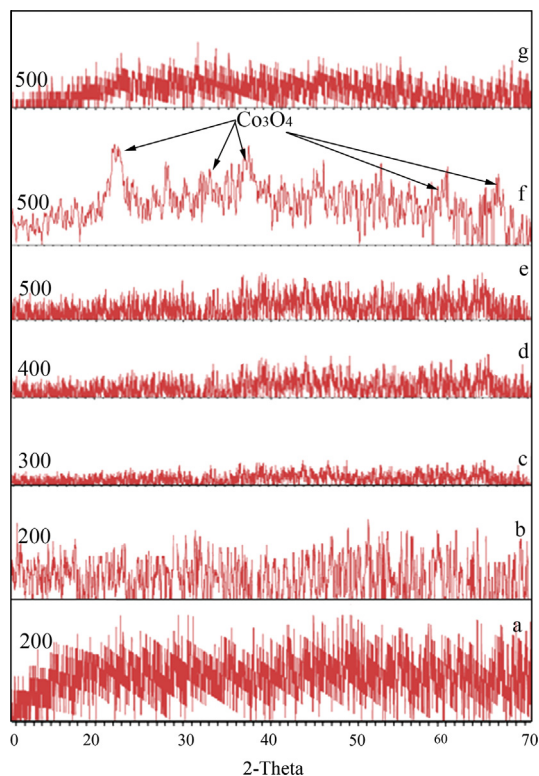


Fig. 2. XRD patterns of (a) Co-B, (b–e) Co-La-Zr-B, (f) Co-B at 500 °C and (g) Co-La-Zr-B at Ar atmosphere.

Table 1
Surface area and elemental analysis of catalysts.

	BET (m ² /g)	EDS ^a	ICP
Co-B	64	–	–
Co-La-Zr-B	123	Co/La: 0.8 Co/Zr: 0.9 La/Zr: 0.8	Co/La: 0.9 Co/Zr: 1.1 La/Zr: 0.7

^a Average from five points in SEM image.

investigation was achieved by EDS pattern. Since EDS pattern only show elemental analysis of one point of catalyst surface, it is not trustworthy. For this reason, five points of catalyst surface were tested for Cobalt, Lanthanum and Zirconium contents. Average results are shown in Table 1. It can be found that EDS data is close to ICP analysis. Fig. 3 shows FE-SEM image of Co-La-Zr-B amorphous nano alloy. As clearly seen, Fig. 3 confirms that there are no agglomerated ultrasound-assisted Co-La-Zr-B nano alloy. If it is not possible to determine the size and morphology of nano alloy by SEM, it is only due to poor ability of scanning electron microscope. EDS pattern of Co-La-Zr-B is shown as inset of Fig. 3. There are three peaks around 2.2, 4.6 and 6.95 keV corresponded to Zr, La and Co, respectively. TEM image of Co-La-Zr-B quaternary amorphous alloy is shown in Fig. 4. It can be seen that, the most of the nanoparticles are in cluster form and also there are several particles had spherical morphology. However, average size of cluster nano alloy is lower than 10 nm.

3.2. Kinetic study of the hydrolysis of NaBH₄ catalyzed by Co-La-Zr-B nano alloy

Fig. 5 shows hydrogen generation of Co-La-Zr-B and Co-B catalyst. As seen, activity of Co-La-Zr-B is higher than Co-B catalyst. It is probably attributed to the BET value of Co-La-Zr-B. As

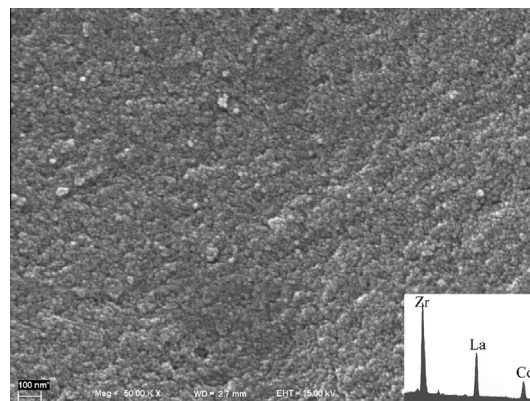


Fig. 3. FE-SEM image of Co-La-Zr-B amorphous nano alloy; inset: EDS pattern.

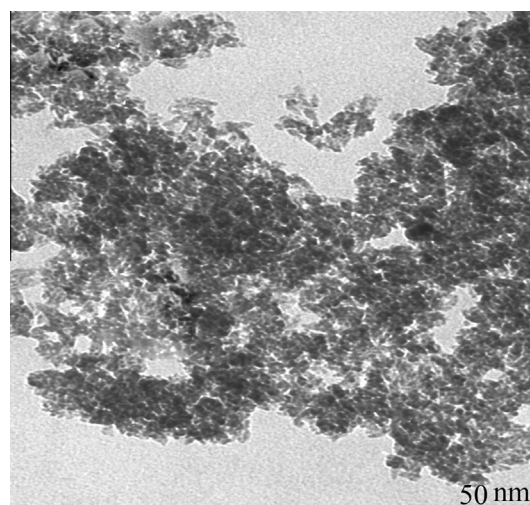


Fig. 4. TEM micrograph of Co-La-Zr-B amorphous nano alloy.

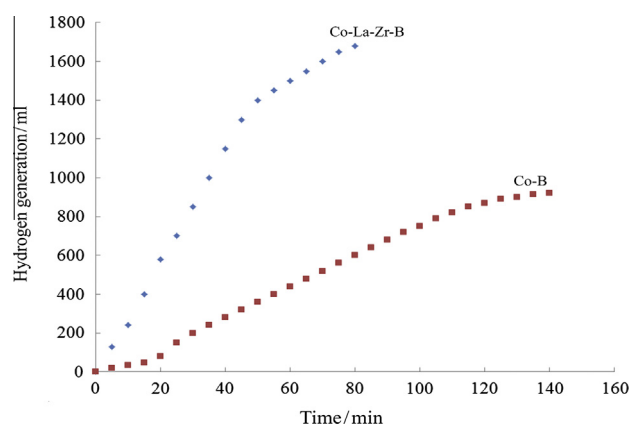


Fig. 5. Hydrogen generation by Co-B and Co-La-Zr-B catalysts.

mentioned already, surface area of Co-La-Zr-B powder is larger than Co-B catalyst. Because of larger surface area and subsequently more active site for hydrolysis of NaBH₄ solution by Co-La-Zr-B powder, it is faster, easier and significant reaction. The kinetics of the hydrolysis of NaBH₄ catalyzed by the Co-La-Zr-B amorphous nano alloy catalyst was studied with regard to the catalyst dosage, initial concentration of sodium borohydride and temperature. Fig. 6a shows the plot of the volume of hydrogen gas generated

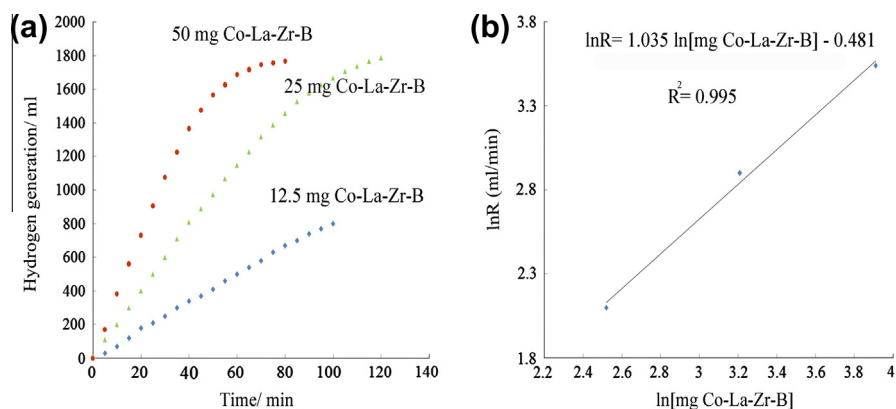


Fig. 6. (a) The volume of hydrogen versus time plot depending on the catalyst dosage at constant sodium borohydride (5 wt%) for the hydrolysis of NaBH₄ catalyzed by Co-La-Zr-B amorphous nano alloy and (b) the plot of hydrogen generation rate versus the catalyst dosage (both in logarithmic scale).

from the hydrolysis of sodium borohydride solution versus time in the presence of different amounts of Co-La-Zr-B catalyst at 40 °C. It is clear that the hydrogen generation rate increases with the catalyst dosage increasing from 12.5 to 50 mg. Fig. 6b shows the plot of the hydrogen generation rate versus the catalyst dosage for the same reaction. The hydrogen generation rate was determined from the linear portion of each plot. The slope (1.035) of the straight line is nearly 1 indicating that the hydrolysis reaction is first order with respect to the amount of Co-La-Zr-B catalyst. Theoretically, higher NaBH₄ concentration is highly desired for achieving high hydrogen capacity, but gets restricted by the solubility limitation of NaBH₄ itself and hydrolysis product NaBO₂ in water [31]. The effect of substrate concentration on hydrogen generation rate was studied by performing a series of experiments starting with varying initial concentrations of NaBH₄ while keeping the catalyst concentration constant at 50 mg Co-La-Zr-B. Fig. 7a shows the volume of hydrogen generated versus time plots depending on the substrate concentrations at constant catalyst concentration. Fig. 7b shows the plot of hydrogen generation rate versus the concentration of substrate. The slope (0.253) of the straight line is nearly zero indicating that the hydrolysis reaction is independent with respect to the initial concentration of NaBH₄. Consequently, the rate law for the catalytic hydrolysis of sodium borohydride can be given as in equation (2),

$$\frac{-4d[\text{NaBH}_4]}{dt} = \frac{d[\text{H}_2]}{dt} = k[\text{Co-La-Zr-B}] \quad (2)$$

Then, the hydrolysis of NaBH₄ catalyzed by Co-La-Zr-B amorphous nano alloy was carried out at the temperatures of 20, 30, 40 and 50 °C starting with the constant initial amounts of sodium borohydride (5 wt%) and Co-La-Zr-B amorphous nano alloy (50 mg).

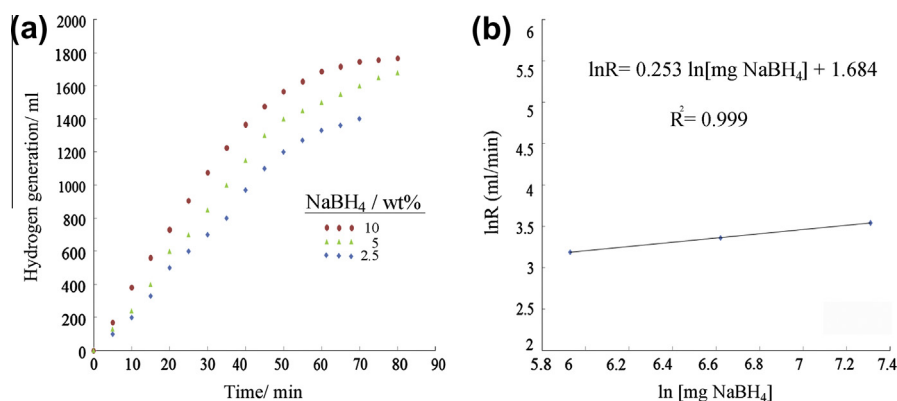


Fig. 7. (a) The volume of hydrogen versus time plot depending on the sodium borohydride at constant catalyst dosage (50 mg) for the hydrolysis of NaBH₄ catalyzed by Co-La-Zr-B amorphous nano alloy and (b) the plot of hydrogen generation rate versus the NaBH₄ concentration (both in logarithmic scale).

Fig. 8a shows the plot of the volume of hydrogen gas generated from the hydrolysis of NaBH₄ solution versus time in the presence of Co-La-Zr-B catalyst at various temperatures. It is clear that the hydrogen generation rate increases from 6.97 to 62.6 ml min⁻¹ with the solution temperature increasing from 293 to 323 K. The rate constants (Table 2) of hydrogen generation from the hydrolysis of NaBH₄ were measured from the linear portions of the plots at three different temperatures and used for the calculation of activation energy from the Arrhenius plot shown in Fig. 8b. The slope of the straight line gives activation energy of 60.06 kJ mol⁻¹, which is lower than the previously reported value, 68.9 kJ mol⁻¹, for Co-B catalyst [32] and slightly higher than 56 kJ mol⁻¹, for Ru supported on IRA-400 [8]. Compared with the activation energies found for NaBH₄ hydrolysis catalyzed with other catalysts (75 kJ mol⁻¹ for Co, 71 kJ mol⁻¹ for Ni [33]), Co-La-Zr-B catalyst shows a lower value, indicating higher catalytic activities for hydrogen generation from hydrolysis of NaBH₄. Mechanism of hydrogen generation through hydrolysis of sodium borohydride is shown in Scheme 2. According to this mechanism, both BH₄⁻ and H₂O adsorb over the catalyst surface sites. However, the adsorption of both reactants implies that the adsorption sites are of different electronic structure. The adsorption sites are certainly atoms on defect sites with different local electronic density. BH₄⁻ should adsorb over electron-rich sites, such as O^{δ-} or Co⁰, which would transfer their electronic density towards the B element. H₂O should adsorb over electron-deficient sites, such as Co^{δ+}, which would attract the electronic density of O of H₂O. It is noteworthy that the nature of the adsorption sites and the nature of the adsorbed hydrolysis intermediates are not well known yet [34]. Stability of Co-La-Zr-B nano alloy was investigated by XRD pattern. After first run reaction, catalyst

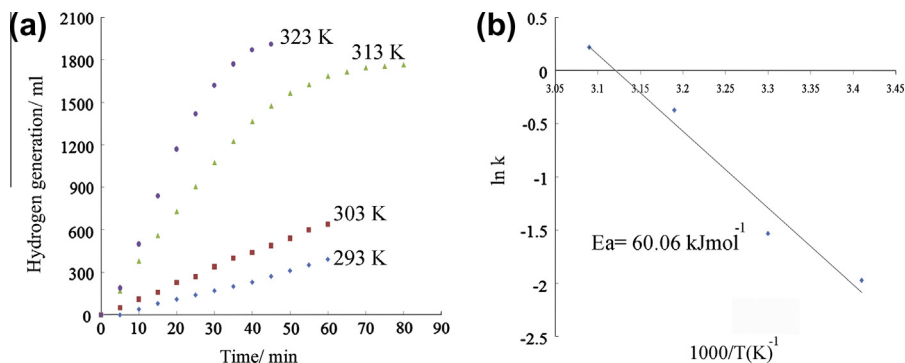
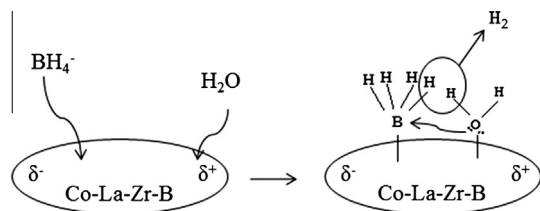


Fig. 8. (a) The volume of hydrogen versus time plot at different temperatures for the hydrolysis of NaBH₄ (5 wt%) catalyzed by Co–La–Zr–B amorphous nano alloy (50 mg) and (b) Arrhenius plot (ln *k* versus the reciprocal absolute temperature 1000/*T* (K⁻¹)).

Table 2

The values of rate constants *k* for the catalytic hydrolysis of sodium borohydride catalyzed by Co–La–Zr–B amorphous nano alloy starting with a solution of 5 wt% NaBH₄ and 50 mg Co–La–Zr–B at different temperatures.

Temperature (K)	Rate constant <i>k</i> for Co–La–Zr–B (ml H ₂) (mg cat) ⁻¹ (min) ⁻¹
293	0.1394
303	0.2164
313	0.6906
323	1.252



Scheme 2. Mechanism of hydrogen generation.

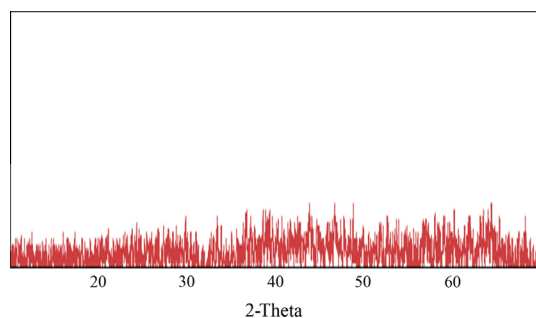


Fig. 9. XRD pattern of recovered Co–La–Zr–B powder.

powder was recovered and washed several times with deionized water and then dried in oven at 50°C. XRD pattern of recovered Co–La–Zr–B catalyst is shown in Fig. 9. It can be seen that, phase structure of catalyst is same to the fresh sample. Indeed, after hydrolysis of NaBH₄ stability of catalyst was not changed.

4. Conclusions

In summary, our study on the preparation and characterization of Co–La–Zr–B quaternary amorphous nano alloy in the hydrolysis

of sodium borohydride led to the following conclusions: Co–La–Zr–B amorphous nano alloy was prepared in aqueous solution under ultrasound irradiation. XRD patterns for several calcination temperatures were recorded and results declared that Co–La–Zr–B nano alloy is amorphous phase and there is no observe any phase of metal oxides under Ar atmosphere. TEM image depicts that amorphous nano alloy is the most of the nanoparticles are in cluster form and also there are several particles had spherical morphology. It is highly active catalyst for hydrogen generation from the hydrolysis of NaBH₄. Activity of Co–La–Zr–B is higher than Co–B catalyst. Kinetic studies show that catalytic hydrolysis of NaBH₄ is first order with respect to the catalyst concentration and zero order respect to the sodium borohydride concentration. Activation energy for the hydrolysis of sodium borohydride in the presence of amorphous Co–La–Zr–B nano alloy, 60.06 kJ mol⁻¹, determined from the evaluation of kinetic data at various temperatures, are smaller than most of the values reported for the same reaction in the presence of other catalyst systems.

Acknowledgment

The authors are grateful to the Research Council of University of Guilan for the partial support of this study.

References

- [1] Z.H. Wang, C.J. Choi, B.K. Kim, J.C. Kim, Z.D. Zhang, J. Alloys Comp. 351 (2003) 319–323.
- [2] D.M.F. Santos, C.A.C. Sequeira, Renewable Sustainable Energy Rev. 15 (2011) 3980–4001.
- [3] H.I. Schlesinger, H.C. Brown, A.E. Finholt, J.R. Gilbreath, H.R. Hoekstra, E.K. Hyde, J. Am. Chem. Soc. 75 (1953) 215–219.
- [4] V.G. Minkina, S.I. Shabunya, V.I. Kalinin, V.V. Martynenko, A.L. Smirnova, Int. J. Hydrogen Energy 33 (2008) 5629–5635.
- [5] S.S. Muir, X. Yao, Int. J. Hydrogen Energy 36 (2011) 5983–5997.
- [6] Y. Bai, C. Wu, F. Wu, B. Yi, Mater. Lett. 60 (2006) 2236–2239.
- [7] G. Guella, C. Zanchetta, B. Patton, A. Miotello, J. Phys. Chem. B 110 (2006) 17024–17033.
- [8] S.C. Amendola, J.M. Janjua, N.C. Spencer, M.T. Kelly, P.J. Petillo, S.L. Sharp-Goldman, M. Binder, Int. J. Hydrogen Energy 25 (2000) 969–975.
- [9] S. Suda, Y.M. Sun, B.H. Liu, Y. Zhou, S. Morimitsu, K. Arai, N. Tsukamoto, M. Uchida, Y. Candra, Z.P. Li, Appl. Phys. A: Mater. Sci. Process. 72 (2001) 209–212.
- [10] B.H. Liu, Z.P. Li, S. Suda, J. Alloys Comp. 415 (2006) 288–293.
- [11] S.U. Jeong, E.A. Cho, S.W. Nam, I.H. Oh, U.H. Jung, S.H. Kim, Int. J. Hydrogen Energy 32 (2007) 1749–1754.
- [12] N. Patel, G. Guella, A. Kale, A. Miotello, B. Patton, C. Zanchetta, L. Mirengi, P. Rotolo, Appl. Catal., A Gen. 323 (2007) 18–24.
- [13] A.H. Uken, C.H. Bartholomew, J. Catal. 65 (1980) 402–415.
- [14] H. Li, Y. Wu, H. Luo, M. Wang, Y. Xu, J. Catal. 214 (2003) 15–25.
- [15] H. Li, H. Li, W.L. Dai, M.H. Qiao, Appl. Catal., A Gen. 238 (2003) 119–130.
- [16] H.X. Li, H. Li, M. Wang, Appl. Catal., A Gen. 207 (2001) 129–137.
- [17] D.S. Lu, W.S. Li, X. Jiang, C.L. Tan, R.H. Zeng, J. Alloys Comp. 485 (2009) 621–626.
- [18] J. Shen, Z. Li, Q. Yan, Y. Chen, J. Phys. Chem. 97 (1993) 8504–8511.
- [19] H. Li, H. Luo, L. Zhuang, W. Dai, M. Qiao, J. Mol. Catal. A: Chem. 203 (2003) 267–275.

- [20] K.S. Suslick, S.B. Choe, A. Cichowlas, M.W. Grinstaff, *Nature* 353 (1991) 414–416.
- [21] P. Mulvaney, R. Cooper, F. Grieser, D. Meisel, *J. Phys. Chem.* 94 (1990) 8339–8345.
- [22] N.A. Dhas, A. Gedanken, *Chem. Mater.* 9 (1997) 3144–3154.
- [23] L.H. Thompson, L.K. Doraiswamy, *Ind. Eng. Chem. Res.* 38 (1999) 1215–1249.
- [24] R. Fernandes, N. Patel, A. Miotello, M. Filippi, *J. Mol. Catal. A: Chem.* 298 (2009) 1–6.
- [25] N. Patel, R. Fernandes, A. Miotello, *J. Power Sources* 188 (2009) 411–420.
- [26] R. Fernandes, N. Patel, A. Miotello, *Int. J. Hydrogen Energy* 34 (2009) 2893–2900.
- [27] R. Fernandes, N. Patel, A. Miotello, *Appl. Catal. B: Environ.* 92 (2009) 68–74.
- [28] Z.Z. Yuan, J.M. Chen, Y. Lu, X.D. Chen, *J. Alloys Comp.* 450 (2008) 245–251.
- [29] M.M. Kreevoy, R.W. Jacobson, *Ventron Alembic* 15 (1979) 2–3.
- [30] C.-Bin Wang, C.-C. Lee, J.-L. Bi, J.-Y. Siang, J.-Y. Liu, C.-T. Yeh, *Catal. Today* 146 (2009) 76–81.
- [31] Y. Liang, H. Dai, L. Ma, P. Wang, H. Cheng, *Int. J. Hydrogen Energy* 35 (2010) 3023–3028.
- [32] S.U. Jeong, R.K. Kim, E.A. Cho, H.J. Kim, S.W. Nam, I.H. Oh, S.A. Hong, S.H. Kim, *J. Power Sources* 144 (2005) 129–134.
- [33] C.M. Kaufman, B. Sen, *J. Chem. Soc., Dalton Trans.* (1985) 307–313.
- [34] J. Andrieuxa, U.B. Demirci, P. Miele, *Catal. Today* 170 (2011) 13–19.